Research Article

Samy Selim, Salem S. Salem*, Medhat E. Owda, Mohammed S. Almuhayawi, Hattan S. Gattan, Mohammed H. Alruhaili, Amna A. Saddiq, Shaimaa Hussein, Mohammad M. Al-Sanea, and Soad K. Al Jaouni*

Biosynthesized zinc oxide nanoparticles: Multifunctional potential applications in anticancer, antibacterial, and *B. subtilis* DNA gyrase docking

https://doi.org/10.1515/gps-2024-0218
received October 07, 2024; accepted January 30, 2025

Abstract: In this work, extracts from okra fruit are used to create zinc oxide nanoparticles (ZnO NPs) in an economical and environmentally friendly manner. During the synthesis process, okra (*Abelmoschus esculentus*) extracts served as stabilizing and reducing agents. Various analytical methods were used to describe the final nanoparticles. The outcomes showed that the produced ZnO NPs primarily exhibited hexagonal shapes, with sizes ranging from 20 to 27 nm in diameter. The cytotoxicity study, conducted on human fibroblast normal HFB4 cell lines, indicated that the IC_{50} dose was 227.8 μg·mL^{-1}. The IC_{50} dose of 119.7 μg·mL^{-1} was found in antitumor effect studies using breast adenocarcinoma Mcf-7 cell lines, revealing a good level of safety for ZnO NPs. Compared to Gram-negative infections, the ZnO NPs were found to have a significantly higher anti-bacterial impact against Gram-positive pathogens. Molecular docking against DNA gyrase A subunit of *Bacillus subtilis* (PDB ID: 4DDQ) illustrated that the ZnO NPs were interlocked with the active site of 4DDQ by a fitting energy value of −50.91 kcal·mol^{-1} through three classical hydrogen bonds with Asp96, Thr220, and Ala221. The last one is also generated by the marketing tromethamine drug (TRS), adding some TRS-like character to the ZnO NP inhibitor.

Keywords: zinc oxide nanoparticles, cytotoxicity, pathogenic bacteria, DNA gyrase A, molecular docking

*** Corresponding author: Salem S. Salem,** Botany and Microbiology Department, Faculty of Science, Al-Azhar University, Nasr City, Cairo, 11884, Egypt, e-mail: salemsalahsalem@azhar.edu.eg
*** Corresponding author: Soad K. Al Jaouni,** Department of Hematology/Oncology, Yousef Abdulatif Jameel Scientific Chair of Prophetic Medicine Application, Faculty of Medicine, King Abdulaziz University, Jeddah, 21589, Saudi Arabia, e-mail: saljaouni@kau.edu.sa
Samy Selim: Department of Clinical Laboratory Sciences, College of Applied Medical Sciences, Jouf University, Sakaka, Saudi Arabia
Medhat E. Owda: Chemistry Department, Faculty of Science, Al-Azhar University, Nasr City, Cairo, 11884, Egypt
Mohammed S. Almuhayawi: Department of Clinical Microbiology and Immunology, Faculty of Medicine, King Abdulaziz University, Jeddah, 21589, Saudi Arabia
Hattan S. Gattan: Department of Medical Laboratory Sciences, Faculty of Applied Medical Sciences, King Abdulaziz University, Jeddah, Saudi Arabia; Special Infectious Agents Unit, King Fahad Medical Research Center, Jeddah, Saudi Arabia
Mohammed H. Alruhaili: Department of Clinical Microbiology and Immunology, Faculty of Medicine, King Abdulaziz University, Jeddah, 21589, Saudi Arabia; Special Infectious Agents Unit, King Fahad Medical Research Center, Jeddah, Saudi Arabia
Amna A. Saddiq: Department of Biological Sciences, Faculty of Science, University of Jeddah, Jeddah 21493, Saudi Arabia
Shaimaa Hussein: Department of Pharmacology, College of Pharmacy, Jouf University, Sakaka, 72341, Aljouf, Saudi Arabia
Mohammad M. Al-Sanea: Department of Pharmaceutical Chemistry, College of Pharmacy, Jouf University, Sakaka, Aljouf, 72341, Saudi Arabia
ORCID: Salem S. Salem 0000-0003-2898-6708

1 Introduction

Research on nanoparticles (NPs) has garnered a lot of focus in the last few years. Nanotechnology is a developing field with the potential for the development of innovative materials and technologies [1,2]. It involves manipulating atoms on the nanoscale to design systems for various purposes. This technology can be applied to create electronic and optical components, nanomaterials, materials science, biotechnology, physics, chemistry, environmental sustainability, hygiene, and new materials used in communication technology [3–8]. Several techniques, such as physical, biological, chemical, and biological approaches, can be used to produce metal oxide nanoparticles, such as sol–gel techniques, thermal decomposition, sonochemical methods, electrochemical processes, microwave radiation, and precipitation [9,10]. Physical methods for

Open Access. © 2025 the author(s), published by De Gruyter. This work is licensed under the Creative Commons Attribution 4.0 International License.

n(NP synthesis require expensive equipment, high temperatures, and high pressure. In contrast, chemical approaches often leave toxic substances on the NPs that harm living organisms and the environment. To address these drawbacks, green synthesis, an eco-friendly approach, has replaced traditional methods. It uses natural molecules from biological tools such as bacteria, plants, algae, and fungi [11–15]. Therefore, recently, the adoption of plant extracts as an eco-friendly and readily available resource for generating biocompatible NPs has attracted the interest of numerous researchers [16–18]. This method offers benefits such as non-toxicity, cost-effectiveness, ease of preparation, and creation of NPs [19–21]. Various plant compounds, particularly flavonoids, contain chemical structures that can interact with metal ions to create NPs. The hydroxyl groups found in flavonoids are especially important in this process, helping to convert metal ions into their NP form [22]. These plant-derived molecules also serve as stabilizing agents for the newly formed nanomaterials, enhancing their compatibility with biological systems and overall stability [23]. The same compounds can facilitate the reduction of metal ions to nanoscale dimensions. In fact, a single step can transform metal ions into nanomaterials using plant-based agents like flavonoids, sterols, alkaloids, and phenols [24]. The specific metal used in green synthesis, along with its properties, largely determines the potential applications of the resulting NPs in various industries [25]. Numerous plant species have been effectively employed by researchers to produce various NPs [26–28]. Zinc oxide nanoparticles (ZnO NPs) are distinct from other metal oxide NPs due to their easily adjustable optical and chemical characteristics brought about by morphological modifications [29]. These NPs exhibit photo-oxidizing and photocatalytic capabilities against both living and non-living concepts [30]. In cutting-edge applications, ZnO NPs are used in various fields [31]. In addition, they hold significant promises for biological sensing and nanomedicine. Notably, durable NPs have even been created by cotton fibers [32]. Research has shown that ZnO NPs can be created using extracts from different plant sources. The plant cells used in the formation process [33] are *Salvia officinalis* [34], *Phyllanthus niruri* [35], *Hibiscus subdariffa* [36], *Tinospora cordifolia* [37], and *Bauhinia variegate* [38]. This research focuses on an environmentally friendly approach for producing ZnO NPs. The method explored here eschews harmful chemicals and streamlines the production process, avoiding complicated laboratory techniques. ZnO NPs were derived from *Abelmoschus esculentus* fruit extract, which acts as an efficient chelating and capping agent. They offer promise due to their unique properties and stability, making them valuable in biomedical fields. Furthermore, *in silico* molecular docking simulations of ZnO NPs with the catalytic domain of *B. subtilis* DNA GyrA (PDB ID: 4DDQ) was also implemented.

2 Materials and methods

2.1 Preparation of *Abelmoschus esculentus* fruit extract

The process of obtaining the okra fruit extract involved several steps. First, the fresh *Abelmoschus esculentus* fruits were washed with deionized water to eliminate any contaminants. Then, they were dehydrated to eliminate any remaining moisture and dust particles. Afterward, about 50 g of the dehydrated *Abelmoschus esculentus* fruits were cut using a stainless-steel knife. These cut fruits were then combined with 100 mL of purified water, forming a mixture. The mixture was stirred for 2 h at a temperature of 60°C to ensure a homogenous solution. The homogenous solution was then centrifuged for 5 min at 1,500 rpm. This process allowed for the separation of the liquid *Abelmoschus esculentus* fruit extract from any solid particles that may have been present. The resulting supernatant, which contained the liquid extract, was then filtered using a filter paper to remove any remaining solid materials. For later use, the filtered extract was stored in a refrigerator for further studies or experiments. This process ensures that the extract is preserved and maintained at the appropriate temperature for analysis and possible applications.

2.2 Green synthesis of ZnO NPs

ZnO NPs are created using the fruit extract from *Abelmoschus esculentus*: 50 mL of the extract is added dropwise to 100 mL of 1 mM zinc acetate while agitating at room temperature. The temperature is then increased to 60°C and maintained for 3 h, during which a white precipitate appears, indicating the formation of ZnO NPs. Centrifugation is used to separate the collected ZnO at 5,000 rpm for 5 min. The procedure is performed twice using purified water and methanol to eliminate the contaminants. The resulting precipitate is calcined at 500°C for 4 h to convert to pure ZnO NPs, as graphically depicted in Figure 1.

2.3 Characterization of the synthesized ZnO NPs

The optical characteristics of ZnO NPs after biosynthesis were characterized using UV-Vis spectroscopy within the wavelength range of 200–800 nm with a Shimadzu UV-1700 spectrophotometer. This technique allows for the assessment

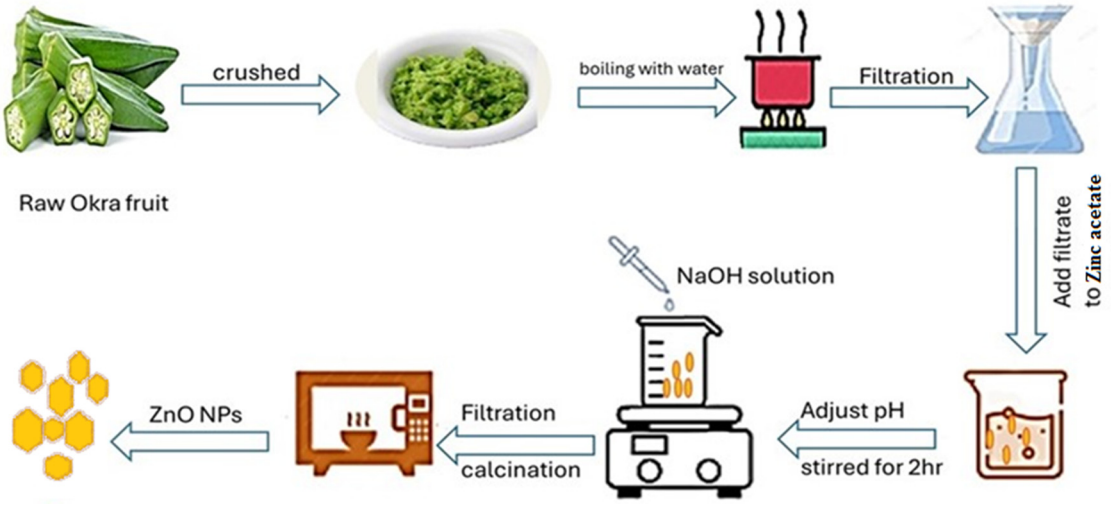

Figure 1: Illustration for ZnO NP production.

of electronic transitions in the NPs, providing insights into their optical behavior.

An Agilent Cary 630 FT-IR spectrometer was used to perform FTIR spectroscopy in the 400–4,000 cm spectrum range in order to determine which functional groups were responsible for the stabilization and reduction of ZnO NPs. KBr was used to prepare the samples for FTIR analysis, which is essential for obtaining clear and interpretable spectra by minimizing the background interference.

To ascertain the crystal form of ZnO NPs, X-ray diffraction (XRD) was performed with a Seifert 3003TT diffractometer employing Cu Kα radiation. This technique gives details on the phase purity and crystallization of the produced NPs.

Transmission electron microscopy (TEM) was employed to examine and evaluate the dimensional characteristics and structural configuration of ZnO NPs. For this investigation, a JEOL (GEM-1010) device was implemented, operating at an electrical potential of 76 kV, allowing for high-resolution imaging of the NPs to assess their size and morphology.

These characterization techniques collectively provide a comprehensive understanding of the synthesized ZnO NPs.

2.4 ZnO NPs cytotoxicity and application as antitumor agent

Cell lines of breast cancer McF-7 and fibroblast normal HFB4 were used to test the cytotoxicity and antitumor properties of ZnO NPs at the Science Way Company (Cairo, Egypt). To form a full monolayer-sheet, 100 µL/well (105 cells/mL) was added to the 96-well culture plate, and it was then incubated for 24 h at 37°C. The growth material was then removed from the 96-well microtiter plates, and the cell layer was washed twice using fresh medium. ZnO NPs were categorized into twofold dilutions in RPMI medium, and the physical characteristics of the layers, such as rounding and shrinkage, were evaluated in multiple wells. Once the mixture was prepared, 20 µL of the MTT mixture was added to each hole. For 5 min, the media were placed on a table that was trembling and shaking at 150 rpm in order to completely integrate the MTT. For 4 h, it was cultivated at 37°C with 5% CO_2 to enable the MTT to metabolize. The formazan was well mixed with the metabolite, allowing it to settle for a short while, and the mixture's spectral density was established at 560 nm.

2.5 Application of ZnO NPs as an antibacterial agent

To assess the biosynthesized antimicrobial qualities of ZnO NPs, four harmful bacteria were used. The following bacteria were cultivated on Mueller–Hinton agar media: *P. aeruginosa, B. subtilis, S. aureus,* and *E. coli.* The inhibitory impact was examined using the well diffusion technique for seven distinct ZnO NP dosages against the four infections. The medium was poured into Petri plates after 0.5 mL of each organism's inoculum had been introduced. The wells were prepared using a 7 mm diameter sterilized cork borer as a standard reference, and 0.1 mL of ZnO NPs at different concentrations (4,000–62.5 µg·mL^{-1}) was then added. Each plate was incubated at 37°C for a full day. The zone of inhibition (IZD) of each plate was calculated using a ruler and expressed as IZD (mm).

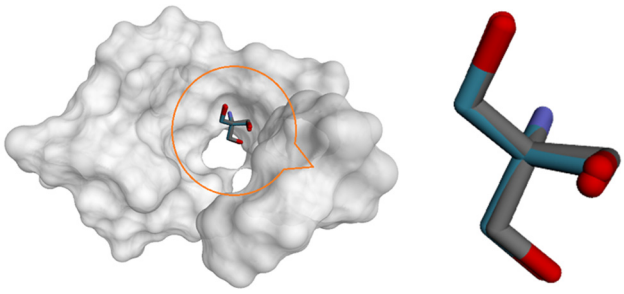

Figure 2: *i*GEMDOCK validation. Crystal TRS (cyan) and the docked one (gray) display similar binding orientation in the binding pocket of 4DDQ with RMSD 0.0240 Å.

2.6 *In silico* molecular docking

According to the previously published protocol [39], a flexible-docking prediction was performed using *i* GEMDOCK app version 2.1. The optimal docking posture of ZnO NPs in the cavity of *B. subtilis* DNA gyrase A (PDB ID: 4DDQ), a significant biological target, was predicted using accurate docking based on a general evolutionary program (GA) and an empirical gaining model. The three-dimensional (3D) structure of 4DDQ complexed with tromethamine (TRS) was downloaded from RCSB Protein Data-Bank (https://www.rcsb.org), and in order to confirm that the docking approach worked, the co-crystallized blocker TRS was removed and re-docked to the appropriate catalytic domain (*i*GEMDOCK validation) (Figure 2). As demonstrated in Figure 2, the docked ligand (TRS) shows the same interaction mode as the crystal one, and the root mean square distance (RMSD) is within the reliable range (0.0240 Å), validating the efficiency of this protocol. After that, the crystallographic information file (CIF) of ZnO NPs was downloaded from the materials project website (https://legacy.materialsproject.org/) and modified using VESTA 3 software [40], saved as pdb format, and finally docked with 4DDQ.

3 Results and discussion

3.1 Visual inspection

A visible color shift and UV-Vis spectral analysis were used to demonstrate the formation of ZnO NPs. The zinc acetate solutions, when added to the extract, turned into a white precipitate, suggesting that the metabolites in the *Abelmoschus esculentus* fruit extract are likely responsible for reducing Zn^{2+} to synthesize ZnO NPs, as shown in Figure 3. Plant metabolites contain numerous functional groups, such as hydroxyl, amine, and carbonyl. These groups have the ability to engage in interactions with metal ions to help reduce them to NP sizes. This process is made possible by the rich array of phytochemicals found in plant extracts, particularly in fruits. These bioactive compounds encompass a wide range of substances, including flavonoids, alkaloids, polyphenols, aldehydes, amides, ketones, vitamins, and carboxylic acids. The presence of these diverse phytochemicals enables plants to help ensure the creation of metal NPs [41].

3.2 UV–Vis analysis

The size and form of metallic NPs have a direct impact on their absorption values. ZnO NPs typically show a sharp, single absorption peak [42]. Phytochemicals in the plant extracts convert metal ions into metal NPs, providing both reducing and stabilizing effects. UV–Vis spectroscopy was

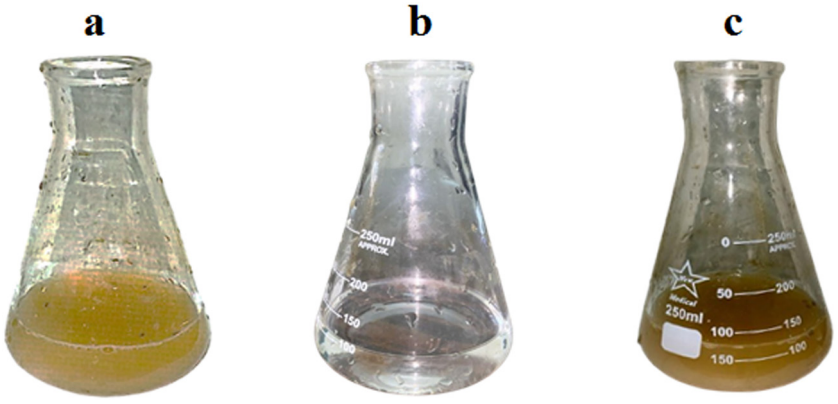

Figure 3: The optical appearance of the ZnO NPs: (a) *Abelmoschus esculentus* extract, (b) zinc acetate, and (c) extract and zinc acetate.

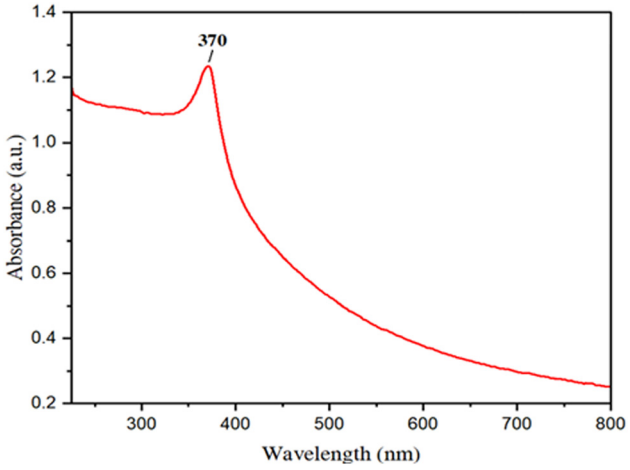

Figure 4: UV–Vis absorption spectrum of ZnO NPs.

utilized to track the reaction's development [43]. Figure 4 illustrates the significant absorption band of ZnO NPs at 370 nm.

3.3 FTIR spectroscopy

The presence of numerous functional groups in the green-synthesized NPs, as detected by FTIR analysis, is shown in Figure 5. According to the existing literature, green-synthesized NPs typically exhibit an organic coating derived from the reducing solution containing flavonoids and phenolic molecules. This coating is believed to enhance the stability and bioactivity of ZnO NPs and other similar NPs. For ZnO NPs, the peaks appearing at 3,442 cm^{-1} are due to the stretching of the OH group, and the peaks at 2,978 and 2,924 cm^{-1} can be attributed to the symmetric and asymmetric stretching of the C–H bond [44]. The peaks at 2,360 and 2,337 cm^{-1} show that CO_2 is formed and may be absorbed through production [45]. The band at 1,637 cm^{-1} is attributed to the C–O stretching vibration of the N acetyl groups of amide-I, the band at 1,549 cm^{-1} is attributed to the amide II group of N–H bending, and the band at 1,436 cm^{-1} for the C–C stretching, and the peak at 1,386 cm^{-1} correlated with the C–O stretching of the COO– group and that at 1,085 cm^{-1} for the stretching of the C–O–C bond [46,47]. The spectral bands observed are linked to various organic compounds present in the Okra fruit extract. These biomolecules, including flavonoids, polyols, and proteins, play crucial roles in both reducing Zn ions to form ZnO NPs and stabilizing the resulting ZnO structures. This phenomenon aligns with the findings from earlier studies on similar biosynthesis processes [48]. The peak at around 900–400 cm^{-1} is typically ascribed to the resonance of the Zn O bonds, indicating the high crystallinity of the synthesized NPs [49,50]. Additionally, the band observed at 667 cm^{-1} is also characteristic of ZnO NPs. Another band formed at 420 cm^{-1} is due to the creation of ZnO NPs, specifically the vibrations of the zinc and oxygen bonds [51,52].

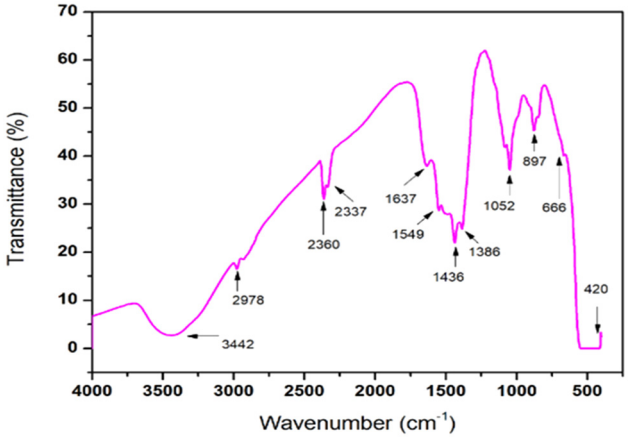

Figure 5: FTIR spectra of the green synthesized ZnO NPs.

3.4 XRD analysis

The XRD patterns of the green-synthesized ZnO NPs using Okra fruit extract are illustrated in Figure 6; they exhibit sharp and well-defined peaks, confirming the hexagonal wurtzite structure of ZnO NPs. The characteristic diffraction peaks were observed at specific 2θ values, which can be indexed to the corresponding lattice planes of the ZnO crystal structure in accordance with the standard JCPDS-card No, 36-1451. These peaks are in accordance with the standard JCPDS card No: 36-1451. These peaks having 2θ values of 1.752°, 34.385°, 36.219°, 47.491°, 56.500°, 62.756°, and 67.838° correspond to the lattice planes 100, 002, 101, 102, 110, 103, and 112, respectively, indicating the successful

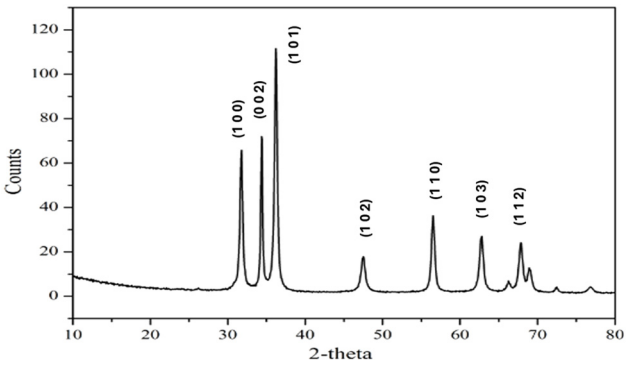

Figure 6: XRD pattern of ZnO NPs.

Table 1: XRD characteristics of the green synthesized ZnO NPs

Angle	*d* value	Net intensity	Relative intensity	FWHM
26.219°	3.39616 Å	74.3951	0.9%	0.142
34.385°	2.60601 Å	5387.30	64.8%	0.154
72.418°	1.30397 Å	173.875	2.1%	0.196
31.752°	2.81591 Å	4714.35	56.7%	0.222
36.219°	2.47815 Å	8317.25	100.0%	0.228
56.500°	1.62745 Å	2700.21	32.5%	0.239
62.756°	1.47940 Å	1868.81	22.5%	0.288
67.838°	1.38042 Å	1731.30	20.8%	0.296
68.945°	1.36092 Å	835.630	10.0%	0.304
53.944°	1.69835 Å	49.9876	0.6%	0.327
47.491°	1.91297 Å	1156.96	13.9%	0.328
76.829°	1.23973 Å	210.631	2.5%	0.336
66.246°	1.40967 Å	354.671	4.3%	0.407
4.195°	3.67558 Å	36.0741	0.4%	0.504

formation of crystalline ZnO NPs using the green method involving Okra fruit extract. The sharp and strong peaks of diffraction devoid of any subsequent phases suggest a significant level of purity and crystals in the synthesized NPs. The Debye–Scherrer formula was used to obtain the average particle size (Table 1):

$$D = k\lambda/\beta\cos\theta$$

where D is the particle size diameter, λ is the wavelength of Cu-Kα radiation in Å, β is the full width at half-maximum, and θ is the Bragg-diffraction angle. Based on the most noticeable typical pattern for the (101) XRD plane, the diameter of ZnO NPs was calculated, and the median size of the particles of the crystallite was found to be around 26.3 nm.

The results indicate that calcination, the process of heating a substance to a high temperature, can produce highly crystalline ZnO NPs with low levels of contaminants. The purity of the resulting nanopowder was confirmed by X-ray diffraction (XRD) analysis, which showed only the characteristic peaks of ZnO NPs without any additional impurity peaks 245. This suggests that the calcination process was effective in obtaining the pure phase of ZnO NPs [53,54].

3.5 TEM-EDX analysis

As shown in Figure 7, the particles appeared to be uniform in size, with an average diameter of 20–27 nm. Some of the particles exhibited a spherical shape, while others had a hexagonal shape, indicating the different crystal structures in ZnO NPs (Figure 7a). The hexagonal particles were found to be smaller in size compared to the spherical ones. Overall, the TEM images provided valuable information about the morphology and size distribution of the pure ZnO NPs. The SAED patterns in Figure 7b show that the ZnO NPs were composed of multiple crystals, indicating that they were polycrystalline in nature. This means that the NPs were made up of many small crystalline structures rather than a single crystal. The particles were homogeneous in size and shape, with a consistent hexagonal form. This observation was further confirmed by TEM analysis [55]. EDX analysis was used in order to explore the composition of the ZnO NP sample, enabling a deeper understanding of its topography. According to EDX analysis (Figure 7c), the primary elements

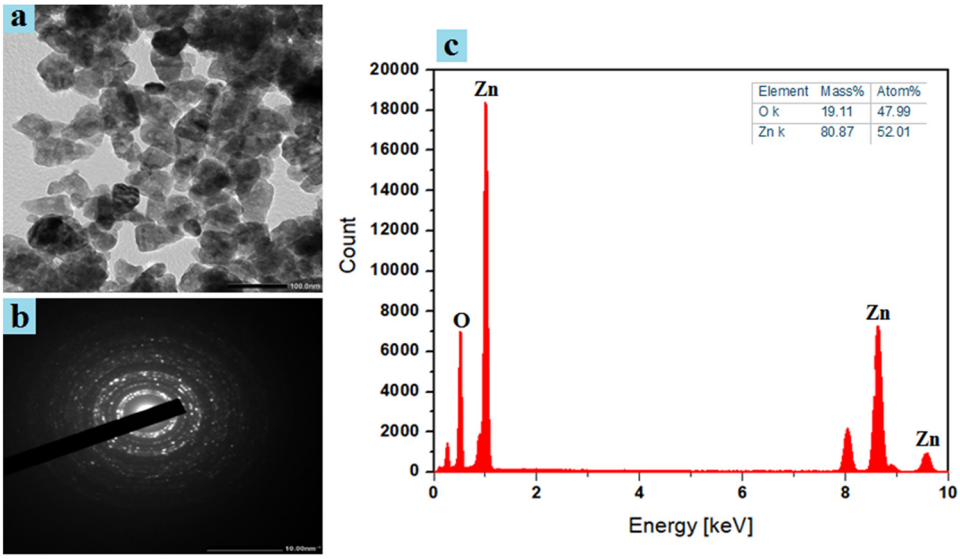

Figure 7: (a) TEM image, (b) SAED, and (c) EDX profile of the green synthesized ZnO NPs.

identified in ZnO NPs were zinc and oxygen. Two robust zinc peaks at 1 and 8.7 keV, as well as a lone oxygen peak at approximately 0.5 keV, were observed, all indicative of ZnO NPs. The increased intensity of the Zn and O peaks suggests the presence of zinc oxide within the sample. The impurity-free NP exhibits promising antimicrobial and antibiofilm activity.

3.6 Cytotoxicity and antitumor properties of ZnO NPs

The biological materials were tested for experimental cytotoxicity against types of normal cells in the initial stage of assessing their safety after being exposed to different concentrations of ZnO NPs (500, 250, 125, 62.5, and 31.25 μg·mL^{-1}). Figure 8a shows microscopic images of the morphological alterations of HFB4 cell lines treated with 1,000–250 μg mL^{-1} ZnO NPs. IC_{50} values were calculated using the curve, which evaluated the pharmacological dosage concentration necessary to cause 50% of cell death. The IC_{50} value of the ZnO NPs produced on HFB4 cell lines was 227.8 μg·mL^{-1}, according to the findings displayed in Figure 8a. ZnO NPs were used in anticancer research against Mcf-7 cell lines at several doses between 1,000 and 31.25 μg·mL^{-1}. NPs had an impact on the vitality of Mcf-7 cell lines, as seen in the microscopic images. Based on the morphological changes observed in Mcf-7 cell lines exposed to 1,000–125 μg·mL^{-1} ZnO NPs, as shown in Figure 8b, it was believed that ZnO NPs had anticancer

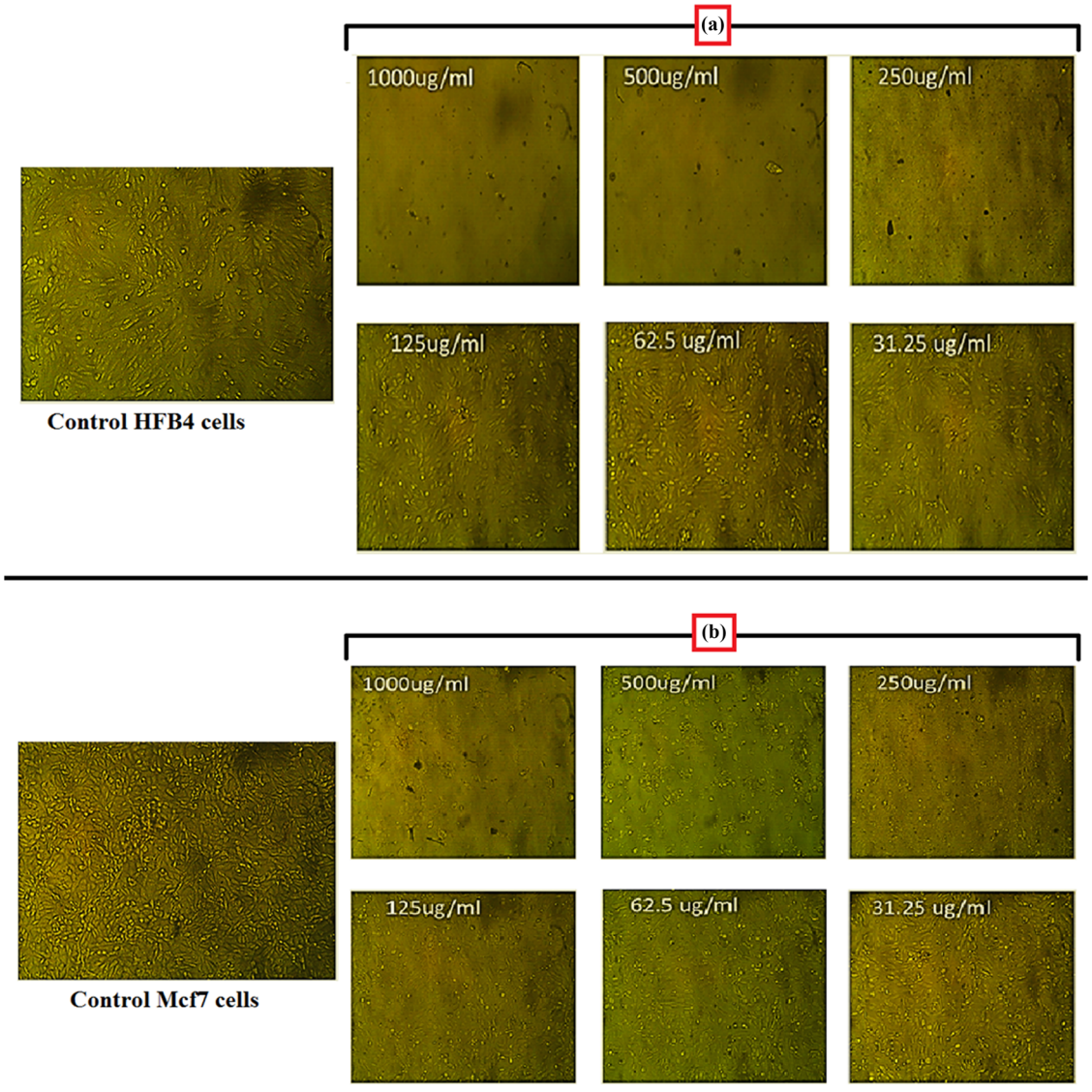

Figure 8: HFB4 (a) and Mcf-7 cell (b) after treatment with ZnO NPs.

effects. ZnO NPs was 119.7 μg·mL^{-1}, as shown in Figure 8b. Previous research also showed that ZnO NPs had higher cell survival at lower concentrations; however, as exposure duration and concentration directly affect cell viability, this varies [56]. Furthermore, the strong anticancer efficacy of the synthesized ZnO NPs targeting cells that cause liver cancer was demonstrated by a greater antiproliferative impact against HepG2 cells at a concentration of 200 μg·mL^{-1}. Previous studies have demonstrated that ZnO NPs effectively inhibit the growth of liver cancer cells [57]. Our findings allow us to conclude that there is clear proof of the anticancer potential of environmentally produced ZnO NPs.

3.7 Application of ZnO NPs as an antibacterial agent

Four pathogenic bacteria, two Gram-positive and the other two Gram-negative, were used to investigate the

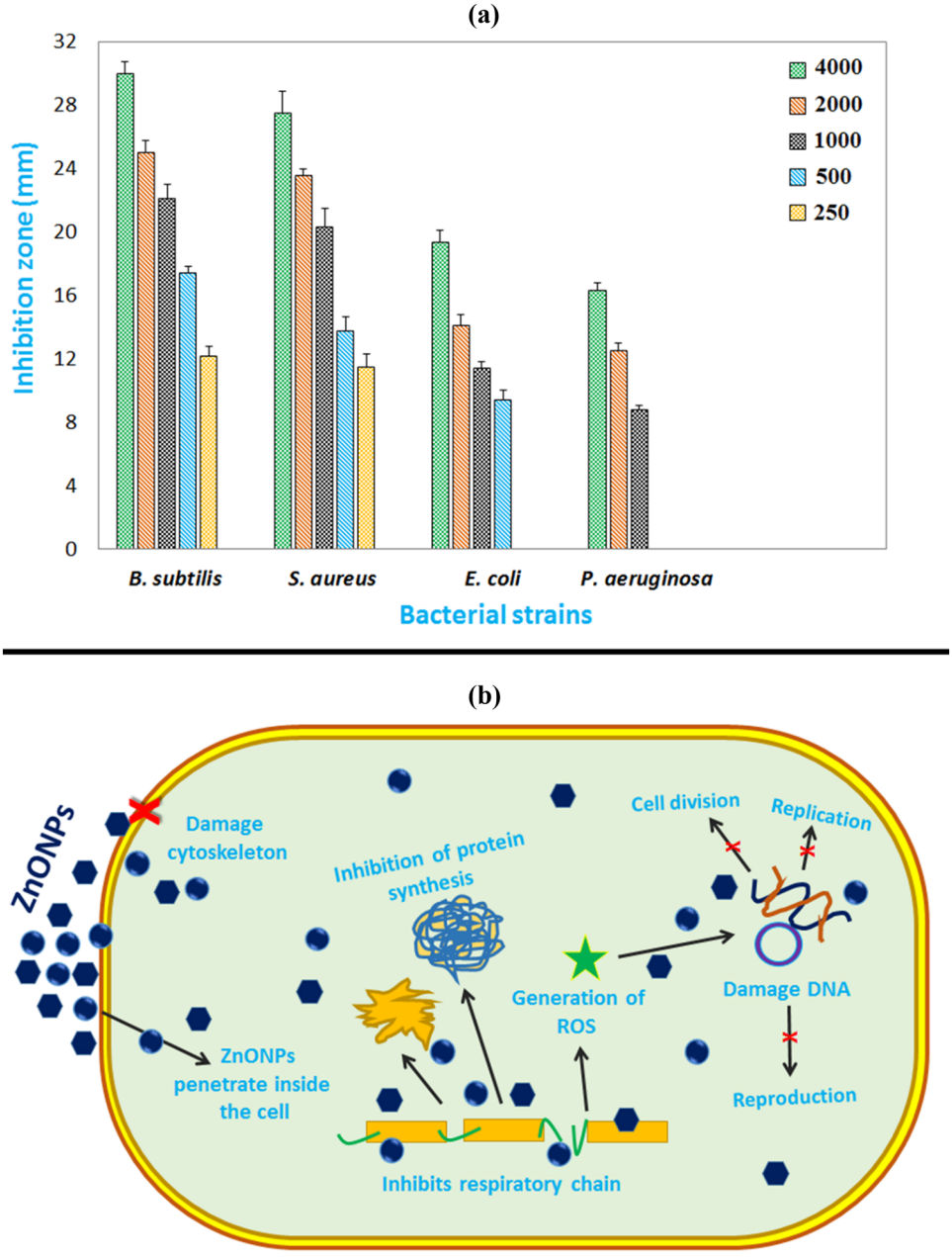

Figure 9: (a) Antimicrobial activity and (b) mechanism diagram for ZnO NPs.

antibacterial susceptibility of the biosynthesized ZnO NPs. Bacteria that are most susceptible were *B. subtilis* and *S. aureus*, with 30 ± 0.8 mm and 27.5 ± 1.4 mm IZD, respectively, based on the data in Figure 9a. In contrast, *E. coli* and *P. aeruginosa* growth were less affected by ZnO NPs, which had the smallest IZD and the lowest vulnerability of 19.4 ± 0.7 and 16.3 ± 0.49 mm, respectively. The results demonstrated that the MIC of ZnO NPs against *B. subtilis* and *S. aureus* microbial growth was superior to that of other strains, with MICs of 250 $\mu g \cdot mL^{-1}$ against both species. Conversely, *E. coli* and *P. aeruginosa* had MICs of 500 and 1,000 $\mu g \cdot mL^{-1}$, respectively. Compared to Gram-negative pathogens, ZnO NPs showed a substantially higher antibacterial impact against Gram-positive pathogens since (Figure 9) they abolished the antibacterial action of Gram-positive infections. According to earlier studies, ZnO NPs interact with bacterial cell membranes to increase their antibacterial action [56]. This is because ZnO NPs have a large specific surface area [58]. ZnO NPs and the cell membrane have more possibilities to exhibit the results, which encourage positive interactions with bacteria and boost activity [59]. ZnO NPs interact negatively with the bacterial cell membranes, causing reactive oxygen species to be produced and the elements that make up the membrane of bacteria to be disrupted or oxidized (Figure 9b) [56]. Furthermore, these findings imply that, in contrast to Gram-negative bacteria, Gram-positive bacteria are more vulnerable to ZnO NPs [46]. The two species of bacteria have different cell wall architectures, which explains this impact. The complex cell wall structure of Gram-negative bacteria includes an outer membrane made of lipopolysaccharides, which acts as an extra barrier against antibacterial drugs [60]. Because of its negative charges, this outer membrane makes the cell wall thicker and prevents antibacterial substances from penetrating the cell, decreasing its efficacy. However, Gram-positive bacteria are more vulnerable to antibacterial drugs due to their simpler cell wall construction [61]. The possible use of ZnO NPs as a substitute for antibacterial drugs in the therapy of bacteria is affected by these findings.

3.8 Molecular docking results of antibacterial target

The results of the antibacterial screening indicate that ZnO NPs had the greatest inhibitory effect on *B. subtilis* with an IZD of 30 ± 0.8 mm (Figure 9). To gain insights into their action mechanism, *in silico* molecular docking was conducted against isomerase *B. subtilis* DNA gyrase A subunit (homodimer), a promising target for antimicrobial agents [62]. A flexible docking simulation of ZnO NPs against 4DDQ (PDB ID) was implemented using the *i*GEMDOCK software version 2.1 [39]. As shown in Figure 10, ZnO NPs fitted into the active site of 4DDQ with a binding energy of $-50.91\ kcal \cdot mol^{-1}$ through hydrogen bonds and electrostatic interactions. The classical H-bonds are generated between the oxygen of ZnO (as acceptors) and hydrogen donors NH and OH groups of amino acid residues, including Asp96, Thr220, and Ala221. It is worth mentioning that the last residue (Ala221, 3.03 Å) is also formed by the interaction between the NH_2 and OH groups of the co-crystallized tromethamine small molecule (TRS) and Ala221 (2.70, 3.17 Å), indicating TRS-like character to the ZnO NP inhibitor. Moreover, another electrostatic interaction (charge-charge) is formed between the Zn atom and negative aspartate (Asp96, 4.43 Å), proving good stabilization of ZnO NPs within the central cavity of 4DDQ. Understanding protein–metal adherence and the network of molecules that results from the interaction of nanomaterials with biomolecules is crucial, and this understanding has led to the development of molecular docking, a tool that can be used to predict the partnership affinity of protein–metal combinations as well as the obstacles and limitations that arise when binding is not possible [63]. In prior work, AutoDock 4.2 was used to molecularly dock copper oxide against vital proteins of *E. coli* and *S. epidermidis*. The findings showed binding energies against the proteins of *E. coli* and *S. epidermidis*, suggesting possible interactions and laying the groundwork for a deeper understanding of the molecular underpinnings of

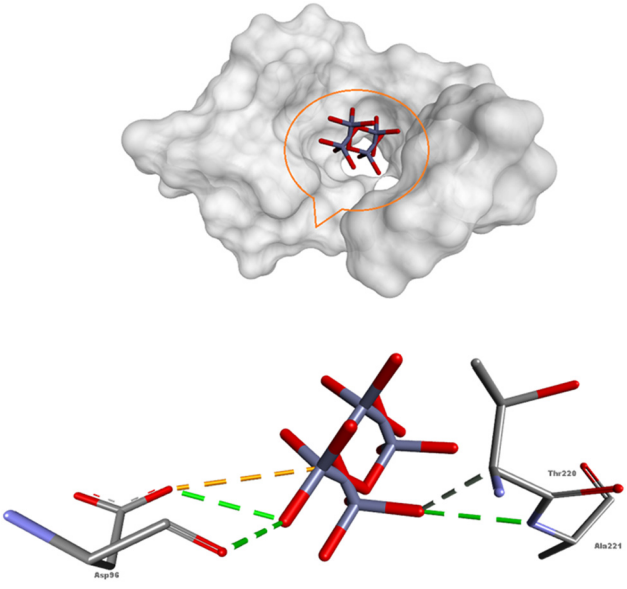

Figure 10: Molecular docking 3D representation of ZnO NPs with the active site of *B. subtilis* DNA gyrase A (PDB ID: 4DDQ).

the spotted antibacterial behavior *in vitro* toward *E. coli* and *S. epidermidis* [64]. Molecular docking has a wide range of yet little-studied applications in the biological use of ZnO NPs.

4 Conclusion

The current study developed a low-cost, environmentally friendly method of producing bio-functionalized ZnO NPs using *Abelmoschus esculentus* fruit extract. To the best of our knowledge, this is the novel work on the green fabrication bioinspired ZnO NPs from *Abelmoschus esculentus* fruit extract, and it also demonstrated the anticancer, antibacterial, and molecular docking properties. Using FTIR, UV-Vis, XRD, EDX, and TEM analyses, the form, architectural, and optical characteristics of the biogenic synthesized ZnO NPs were investigated. The existence of a significant absorbance band at 370 nm and XRD peaks that matched crystalline monoclinic ZnO NPs perfectly validated the creation of ZnO NPs. The distorted, mostly hexagonal with average sizes of 20–27 nm were visible using the TEM method. The appearance of solely Zn and O peaks in the EDX analysis verified the purity of the nanomaterial. The susceptibility of bacterial pathogens versus ZnO NPs was also observed with MICs of 250 $\mu g \cdot mL^{-1}$ for *B. subtilis* and *S. aureus*, while it was 1,000 and 500 $\mu g \cdot mL^{-1}$ for *P. aeruginosa* and *E. coli*, respectively. Nevertheless, their greatest anticancer effect was seen against Mcf-7, and IC_{50} was 119.7 $\mu g \cdot mL^{-1}$. Molecular docking proved the ability of ZnO NPs to be a good inhibitor of DNA gyrase A; thus, it is considered a powerful antimicrobial agent against *B. subtilis*. Overall, the findings confirmed that ZnO NPs fabricated employing the extract of Okra fruit have the potential to be used as active agents in various biomedical applications after further detailed clinical investigations.

Acknowledgments: The authors extend their appreciation to the Deanship of Graduate Studies and Scientific Research at Jouf University.

Author contributions: Samy Selim: investigation, writing – original draft preparation, and funding acquisition. Salem S. Salem and Medhat E. Owda: conceptualization, validation, methodology, data curation, formal analysis, investigation, writing – original draft preparation, and writing – review and editing Mohammed S. Almuhayawi, Hattan S. Gattan, Mohammed H. Alruhaili, Amna A. Saddiq, Shaimaa Hussein, Mohammad M. Al-Sanea, and Soad K. Al Jaouni: data curation, formal analysis, investigation, writing – review and editing and funding acquisition.

Conflict of interest: The authors state no conflict of interest.

Data availability statement: The datasets generated during and/or analyzed during the current study are available from the corresponding author on reasonable request.

References

[1] Tokas R, Bhardwaj LK, Kumar N, Jindal T. Nanotechnology for sustainable development and future: A review. Green and sustainable approaches using wastes for the production of multifunctional nanomaterials. Netherlands: Elsevier; 2024. p. 221–33.
[2] Salem SS. A mini review on green nanotechnology and its development in biological effects. Arch Microbiol. 2023;205:128.
[3] Mekuye B, Abera B. Nanomaterials: An overview of synthesis, classification, characterization, and applications. Nano Sel. 2023;4:486–501.
[4] Altammar KA. A review on nanoparticles: characteristics, synthesis, applications, and challenges. Front Microbiol. 2023;14:1155622.
[5] Alabssawy AN, Abu-Elghait M, Azab AM, Khalaf-Allah HM, Ashry AS, Ali AO, et al. Hindering the biofilm of microbial pathogens and cancer cell lines development using silver nanoparticles synthesized by epidermal mucus proteins from Clarias gariepinus. BMC Biotechnol. 2024;24:28.
[6] Dezfuli AAZ, Abu-Elghait M, Salem SS. Recent insights into nanotechnology in colorectal cancer. Appl Biochem Biotechnol. 2024;196:4457–71.
[7] Salem SS. Application of nano-materials. In: Raja R, Hemaiswarya S, Narayanan M, Kandasamy S, Jayappriyan KR, editors. Haematococcus: Biochemistry, biotechnology and biomedical applications. Singapore: Springer Nature Singapore; 2023. p. 149–63.
[8] Elfadel RG, Refat HM, El-Wahab HA, Salem SS, Owda ME, Abdel Reheim MA. Preparation of new surface coating based on modified oil-based polymers blended with ZnO and CuZnO NPs for steel protection. Sci Rep. 2023;13:7268.
[9] Salem SS, Hammad EN, Mohamed AA, El-Dougdoug W. A comprehensive review of nanomaterials: Types, synthesis, characterization, and applications. Biointerface Res Appl Chem. 2023;13:41.
[10] Jadoun S, Arif R, Jangid NK, Meena RK. Green synthesis of nanoparticles using plant extracts: A review. Environ Chem Lett. 2021;19:355–74.
[11] Salem SS. Baker's yeast-mediated silver nanoparticles: Characterisation and antimicrobial biogenic tool for suppressing pathogenic microbes. BioNanoScience. 2022;12:1220–9.
[12] Kalaiyarasi C, Poonkothai M, Abirami S, Alaguprathana M, Marraiki N, Zaghloul NS. Zinc oxide nanoparticles fabrication using Moringa oleifera Lam. seed extract—impact on phytotoxic, photocatalytic, and antimicrobial activities. Appl Nanosci. 2023;13:2187–97.
[13] Soliman MKY, Hashem AH, Al-Askar AA, AbdElgayed G, Salem SS. Green synthesis of silver nanoparticles from Bauhinia variegata and their biological applications. Green Process Synth. 2024;13.
[14] Abd-Elkhalek HF, Badawy AA, Al-Askar AA, Abd Elgawad H, Hashem AH, Salem SS. Biosynthesis and characterization of selenium and silver nanoparticles using Trichoderma viride filtrate and their impact on Culex pipiens. Green Process Synth. 2024;13.

[15] Salem SS. Bio-fabrication of selenium nanoparticles using baker's yeast extract and its antimicrobial efficacy on food borne pathogens. Appl Biochem Biotechnol. 2022;194:1898–910.
[16] Adeyemi JO, Oriola AO, Onwudiwe DC, Oyedeji AO. Plant extracts mediated metal-based nanoparticles: synthesis and biological applications. Biomolecules. 2022;12:627.
[17] Soliman MKY, Amin MA-A, Nowwar AI, Hendy MH, Salem SS. Green synthesis of selenium nanoparticles from Cassia javanica flowers extract and their medical and agricultural applications. Sci Rep. 2024;14:26775.
[18] Ashour EA, Aldhalmi AK, Kamal M, Salem SS, Mahgoub SA, Alqhtani AH, et al. The efficacy of Artichoke leaf extract conjugated with organic zinc nanoparticles on growth, carcass traits and blood biochemical parameters of broilers. Poult Sci. 2024;104:104521.
[19] Ullah A, Lim SI. Plant extract-based synthesis of metallic nanomaterials, their applications, and safety concerns. Biotechnol Bioeng. 2022;119:2273–304.
[20] Aminuzzaman M, Ng PS, Goh W-S, Ogawa S, Watanabe A. Value-adding to dragon fruit (Hylocereus polyrhizus) peel biowaste: Green synthesis of ZnO nanoparticles and their characterization. Inorg Nano-Metal Chem. 2019;49:401–11.
[21] Aminuzzaman M, Ying LP, Goh W-S, Watanabe A. Green synthesis of zinc oxide nanoparticles using aqueous extract of Garcinia mangostana fruit pericarp and their photocatalytic activity. Bull Mater Sci. 2018;41:1–10.
[22] Naseer M, Aslam U, Khalid B, Chen B. Green route to synthesize Zinc Oxide Nanoparticles using leaf extracts of Cassia fistula and Melia azadarach and their antibacterial potential. Sci Rep. 2020;10:9055.
[23] Ettadili F, Aghris S, Laghrib F, Farahi A, Saqrane S, Bakasse M, et al. Recent advances in the nanoparticles synthesis using plant extract: Applications and future recommendations. J Mol Struct. 2022;1248:131538.
[24] Nguyen NTT, Nguyen LM, Nguyen TTT, Nguyen TT, et al. Formation, antimicrobial activity, and biomedical performance of plant-based nanoparticles: A review. Environ Chem Lett. 2022;20:2531–71.
[25] Salem SS, Fouda A. Green synthesis of metallic nanoparticles and their prospective biotechnological applications: An Overview. Biol Trace Elem Res. 2021;199:344–70.
[26] Said A, Abu-Elghait M, Atta HM, Salem SS. Antibacterial activity of green synthesized silver nanoparticles using Lawsonia inermis against common pathogens from urinary tract infection. Appl Biochem Biotechnol. 2024;196:85–98.
[27] Al-Zahrani FAM, Salem SS, Al-Ghamdi HA, Nhari LM, Lin L, El-Shishtawy RM. Green synthesis and antibacterial activity of Ag/Fe_2O_3 nanocomposite using Buddleja lindleyana extract. Bioengineering. 2022;9:452.
[28] ELhabal SF, Elwy HM, Hassanin S, El-Rashedy AA, Hamza AA, Khasawneh MA. Biosynthesis and characterization of gold and copper nanoparticles from Salvadora persica fruit extracts and their biological properties. Int J Nanomed. 2022;17:6095.
[29] Sharma D, Rajput J, Kaith B, Kaur M, Sharma S. Synthesis of ZnO nanoparticles and study of their antibacterial and antifungal properties. Thin solid Films. 2010;519:1224–9.
[30] Hussein J, El-Banna M, Razik TA, El-Naggar ME. Biocompatible zinc oxide nanocrystals stabilized via hydroxyethyl cellulose for mitigation of diabetic complications. Int J Biol Macromol. 2018;107:748–54.
[31] Wang L, Kang Y, Liu X, Zhang S, Huang W, Wang S. ZnO nanorod gas sensor for ethanol detection. Sens Actuators B: Chem. 2012;162:237–43.
[32] Cross SE, Innes B, Roberts MS, Tsuzuki T, Robertson TA, McCormick P. Human skin penetration of sunscreen nanoparticles: in-vitro assessment of a novel micronized zinc oxide formulation. Skin Pharmacol Physiol. 2007;20:148–54.
[33] Ifeanyichukwu UL, Fayemi OE, Ateba CN. Green synthesis of zinc oxide nanoparticles from pomegranate (Punica granatum) extracts and characterization of their antibacterial activity. Molecules. 2020;25:4521.
[34] Abomuti MA, Danish EY, Firoz A, Hasan N, Malik MA. Green synthesis of zinc oxide nanoparticles using salvia officinalis leaf extract and their photocatalytic and antifungal activities. Biology. 2021;10:1075.
[35] Ramesh P, Rajendran A, Ashokkumar M. Biosynthesis of zinc oxide nanoparticles from Phyllanthus Niruri plant extract for photocatalytic and antioxidant activities. Int J Environ Anal Chem. 2024;104:1561–72.
[36] Chemingui H, Moulahi A, Missaoui T, Al-Marri AH, Hafiane A. A novel green preparation of zinc oxide nanoparticles with Hibiscus sabdariffa L.: photocatalytic performance, evaluation of antioxidant and antibacterial activity. Environ Technol. 2024;45:926–44.
[37] Sharma R, Sharma R, Singh RR, Kumari A. Evaluation of biogenic zinc oxide nanoparticles from Tinospora cordifolia stem extract for photocatalytic, anti-microbial, and antifungal activities. Mater Chem Phys. 2023;297:127382.
[38] Singh D, Verma R, Singh KR, Srivastava M, Singh RP, Singh J. Biogenic synthesis of CuO/ZnO nanocomposite from Bauhinia variegate flower extract for highly sensitive electrochemical detection of vitamin B2. Biomater Adv. 2024;161:213898.
[39] Hsu K-C, Chen Y-F, Lin S-R, Yang J-M. iGEMDOCK: A graphical environment of enhancing GEMDOCK using pharmacological interactions and post-screening analysis. BMC Bioinforma. 2011;12:1–11.
[40] Momma K, Izumi F. VESTA 3 for three-dimensional visualization of crystal, volumetric and morphology data. J Appl Crystallogr. 2011;44:1272–6.
[41] Nethravathi P, Shruthi G, Suresh D, Nagabhushana H, Sharma S. Garcinia xanthochymus mediated green synthesis of ZnO nanoparticles: photoluminescence, photocatalytic and antioxidant activity studies. Ceram Int. 2015;41:8680–7.
[42] Meena PL, Poswal K, Surela AK. Facile synthesis of ZnO nanoparticles for the effective photodegradation of malachite green dye in aqueous solution. Water Environ J. 2022;36:513–24.
[43] Abdelmigid HM, Morsi MM, Hussien NA, Alyamani AA, Alhuthal NA, Albukhaty S. Green synthesis of phosphorous-containing hydroxyapatite nanoparticles (nHAP) as a novel nano-fertilizer: preliminary assessment on pomegranate (Punica granatum L.). Nanomaterials. 2022;12:1527.
[44] Hu D, Si W, Qin W, Jiao J, Li X, Gu X, et al. Cucurbita pepo leaf extract induced synthesis of zinc oxide nanoparticles, characterization for the treatment of femoral fracture. J Photochem Photobiol B: Biol. 2019;195:12–6.
[45] Devi TR, Gayathri S. FTIR and FT-Raman spectral analysis of paclitaxel drugs. Int J Pharm Sci Rev Res. 2010;2:106–10.
[46] Abdelghany TM, Al-Rajhi AM, Yahya R, Bakri MM, Al Abboud MA, Yahya R, et al. Phytofabrication of zinc oxide nanoparticles with

advanced characterization and its antioxidant, anticancer, and antimicrobial activity against pathogenic microorganisms. Biomass Convers Biorefin. 2023;13:417–30.
[47] Aadnan I, Zegaoui O, Daou I, da Silva JCE. Synthesis and physico-chemical characterization of a ZnO-Chitosan hybrid-biocomposite used as an environmentally friendly photocatalyst under UV-A and visible light irradiations. J Environ Chem Eng. 2020;8:104260.
[48] Huang Y, Haw CY, Zheng Z, Kang J, Zheng JC, Wang HQ. Biosynthesis of zinc oxide nanomaterials from plant extracts and future green prospects: a topical review. Adv Sustain Syst. 2021;5:2000266.
[49] Selim YA, Azb MA, Ragab I, HM Abd El-Azim M. Green synthesis of zinc oxide nanoparticles using aqueous extract of Deverra tortuosa and their cytotoxic activities. Sci Rep. 2020;10:3445.
[50] Sharmila G, Thirumarimurugan M, Muthukumaran C. Green synthesis of ZnO nanoparticles using Tecoma castanifolia leaf extract: Characterization and evaluation of its antioxidant, bactericidal and anticancer activities. Microchem J. 2019;145:578–87.
[51] Yuvakkumar R, Suresh J, Saravanakumar B, Nathanael AJ, Hong SI, Rajendran V. Rambutan peels promoted biomimetic synthesis of bioinspired zinc oxide nanochains for biomedical applications. Spectrochim Acta Part A: Mol Biomol Spectrosc. 2015;137:250–8.
[52] Balcha A, Yadav OP, Dey T. Photocatalytic degradation of methylene blue dye by zinc oxide nanoparticles obtained from precipitation and sol-gel methods. Environ Sci Pollut Res. 2016;23:25485–93.
[53] Gur T, Meydan I, Seckin H, Bekmezci M, Sen F. Green synthesis, characterization and bioactivity of biogenic zinc oxide nanoparticles. Environ Res. 2022;204:111897.
[54] Lei Y, Qu F, Wu X. Assembling ZnO nanorods into microflowers through a facile solution strategy: morphology control and cathodoluminescence properties. Nano-Micro Lett. 2012;4:45–51.
[55] Kołodziejczak-Radzimska A, Markiewicz E, Jesionowski T. Structural characterisation of ZnO particles obtained by the emulsion precipitation method. J Nanomater. 2012;2012:656353.
[56] Almuhayawi MS, Alruhaili MH, Soliman MK, Tarabulsi MK, Ashy RA, Saddiq AA, et al. Investigating the in vitro antibacterial, antibiofilm, antioxidant, anticancer and antiviral activities of zinc oxide nanoparticles biofabricated from Cassia javanica. PLoS One. 2024;19:e0310927.
[57] Abbasi BH, Shah M, Hashmi SS, Nazir M, Naz S, Ahmad W, et al. Green bio-assisted synthesis, characterization and biological evaluation of biocompatible ZnO NPs synthesized from different tissues of milk thistle (Silybum marianum). Nanomaterials. 2019;9:1171.
[58] Król A, Railean-Plugaru V, Pomastowski P, Buszewski B. Phytochemical investigation of Medicago sativa L. extract and its potential as a safe source for the synthesis of ZnO nanoparticles: The proposed mechanism of formation and antimicrobial activity. Phytochem Lett. 2019;31:170–80.
[59] El-Khawaga AM, Elsayed MA, Gobara M, Suliman AA, Hashem AH, Zaher AA, et al. Correction to: Green synthesized ZnO nanoparticles by Saccharomyces cerevisiae and their antibacterial activity and photocatalytic degradation. Biomass Convers Biorefin. 2025;15:2685. doi: 10.1007/s13399-023-05131-7.
[60] Turner RD, Hurd AF, Cadby A, Hobbs JK, Foster SJ. Cell wall elongation mode in Gram-negative bacteria is determined by peptidoglycan architecture. Nat Commun. 2013;4:1496.
[61] Pasquina-Lemonche L, Burns J, Turner R, Kumar S, Tank R, Mullin N, et al. The architecture of the Gram-positive bacterial cell wall. Nature. 2020;582:294–7.
[62] Rudolph MG, Klostermeier D. Mapping the spectrum of conformational states of the DNA-and C-gates in Bacillus subtilis gyrase. J Mol Biol. 2013;425:2632–40.
[63] Khan T, Lawrence AJ, Azad I, Raza S, Khan AR. Molecular docking simulation with special reference to flexible docking approach. JSM Chem. 2018;6:1053–7.
[64] Álvarez-Chimal R, García-Pérez VI, Álvarez-Pérez MA, Tavera-Hernández R, Reyes-Carmona L, Martínez-Hernández M, et al. Influence of the particle size on the antibacterial activity of green synthesized zinc oxide nanoparticles using Dysphania ambrosioides extract, supported by molecular docking analysis. Arab J Chem. 2022;15:103804.